Available online at www.sciencedirect.com
ScienceDirect
Carbohydrate Polymers 72 (2008) 151–159
Carbohydrate Polymers
www.elsevier.com/locate/carbpol

# Phase segregation of amylopectin and β-lactoglobulin in aqueous system

Carmen Carla Quiroga [a,b,*], Björn Bergenståhl [a]

[a] Division of Food Technology, Lund University, P.O. Box 124, S-221 00 Lund, Sweden
[b] Food and Natural Products Center, San Simon University, P.O. Box 353, Cochabamba, Bolivia

Received 14 April 2007; received in revised form 27 July 2007; accepted 31 July 2007
Available online 19 August 2007

**Abstract**

Phase behavior of aqueous amylopectin and β-lactoglobulin system was studied using Fourier transform infrared spectroscopy. Polysaccharide–protein mixtures were prepared at different concentrations and left for equilibration; afterwards their spectra were recorded and correlated using Partial Least Square analysis. Tertiary phase diagrams were built for the system at different equilibration times (2 and 6 weeks); the binodals were asymmetric and displayed toward the protein concentration. In the two-phase region of the phase diagrams the mixtures showed an upper layer rich in β-lactoglobulin and a lower layer rich in retrograded amylopectin, and in some cases an intermediate layer was seen which was a metastable phase.


*Keywords:* Phase segregation; Phase diagram; Polymer incompatibility; Fourier transform infrared spectroscopy; Amylopectin; β-Lactoglobulin

## 1. Introduction

Polysaccharides and proteins are present together in almost all food systems, therefore, the knowledge of their interactions is of great importance not only because it will help us understand their stability and how they contribute to the structural and textural characteristics of many food systems, but also how we can control these characteristics.

The compatibility between macromolecules depends on macromolecule–macromolecule and macromolecule–solvent interaction forces relative to the entropy of mixing. Polysaccharide–protein mixtures have a limited miscibility due to their high molecular weights and thus the mixing entropy becomes comparably small, therefore, phase separation is a phenomenon which is quite likely to be encountered (Grinberg & Tolstoguzov, 1997; Tolstoguzov, 1986: chap. 9, 1993). Phase separation can be associative or segregative (Piculell, Bergfeldt, & Nilsson, 1995, chap. 2); in an associative phase separation both macromolecules are enriched in one of the separate phases mainly due to intermolecular interactions, most commonly electrostatic attraction, that leads to polysaccharide–protein complex formation, whereas in a segregative phase separation, the two polymers are enriched in separate phases.

A phase separation could be desirable, but it could also be considered an unwanted side-effect. However, regardless of whether a phase separation is wanted to be achieved or avoided, it is essential to know something about the polysaccharide–protein mechanisms that gives rise to phase behavior.

Amylopectin (AP) and β-lactoglobulin (βlg) are widely used in the food industry, yet few studies have been done on this polysaccharide–protein system, and its mechanism of interaction has not yet been fully explained in spite of its industrial significance. Available studies have focused on the relationship between structural parameters and rheological behavior in the AP–βlg particulate gel system (Olsson, Frigaard, Andersson, & Hermansson, 2003; Olsson, Langton, & Hermansson, 2002). However, there is no phase diagram describing the phase behavior of AP–βlg, and only a few AP–protein and polysaccharide–βlg phase diagrams are available, e.g. AP–Casein (Antonov, Grinberg, & Tolstoguzov, 1977), AP–Gelatin (Durrani, Pry-

* Corresponding author. Address: Division of Food Technology, Lund University, P.O. Box 124, S-221 00 Lund, Sweden. Tel.: +46 46 2228307; fax: +46 46 2224622.
*E-mail address:* carla.quiroga@food.lth.se (C.C. Quiroga).

0144-8617/$ - see front matter © 2007 Elsevier Ltd. All rights reserved.
doi:10.1016/j.carbpol.2007.07.041

stupa, Donald, & Clark, 1993; Grinberg & Tolstoguzov, 1972) guar/dextran–βlg (Simonet, Garnier, & Doublier, 2000), and dextran/carrageenan/dextran sulfate–βlg (Zhang & Foegeding, 2003).

Phase separation phenomena have been studied using many techniques, including cloud-point determination, light scattering, thermal analysis, differential scanning calorimetry, microcalorimetry, rheology, fluorescence, nuclear magnetic resonance, and microscopy. Donald, Durrani, Jones, Rennie, and Tromp (1995, chap. 6) have developed an interesting technique, FT-IR spectroscopy, for studying phase behavior. This technique does not require specific staining, it is non-destructive and it is suitable over a wide range of water contents. The only proviso is that the molecules which are studied must show sufficient spectral difference. It can also be used to investigate the effect of temperature, pH, and ionic strength on the phase diagram, and water partitioning as well.

In this study, an AP–βlg–$D_2O$ system was investigated in terms of phase behavior and phase composition and liquid–liquid phase separation kinetics using FT-IR spectroscopy. The main objectives were (i) to build a phase diagram, (ii) to describe the solvent partitioning in the phases, (iii) to find the threshold for phase separation, and (iv) to find out the structure of the phases.

Amylopectin is present in all starches. It is a very large and highly branched polymer with linear chains of (1 → 4)-linked α-D-glucopyranosyl units and α-D-(1 → 6) branches every 24–30 glucose units, constituting 4–5% of the total linkages. The branches of amylopectin molecules are clustered as double helices. Its molecular weight is between $10^7$ and $5 \cdot 10^8$ Da (Manners, 1989).

β-Lactoglobulin is one of the main components of whey protein with a molecular weight of 18,300 Da and an isoelectric point of 5.2, and each monomer consists of 162 amino acid residues. β-Lactoglobulin conformation is strongly dependent on pH, temperature, ionic strength, and concentration (Sawyer, 2003, chap. 7).

## 2. Materials and methods

### 2.1. Materials

Amylopectin was bought from Sigma (No. A-7780, an unmodified, waxy maize starch extracted from a hybrid corn grain with a molecular weight of 20 millon) and deuterium oxide ($D_2O$) from Aldrich (CAS 7789-20, 99.9 atom % D of purity). β-Lactoglobulin was kindly supplied by Arla Foods (PSDI 2400).

### 2.2. Sample preparation

A solution of 15% AP was made by dissolving the polysaccharide in $D_2O$ at 120 °C for 1 h and a solution of 30% βlg was prepared by dissolving the protein in $D_2O$ at room temperature. These solutions (''stock solutions'') were centrifuged at 20,000 r.p.m. for 1 h in order to get rid of the insoluble or contaminant material present in the solutions, the dry matter content after centrifugation was recalculated by gravimetric analysis (a fixed amount of sample was weighed and dried at 105 °C until constant weight was obtained); the final AP and βlg concentration were around 14% and 28%, respectively.

The stock solutions were used for preparing AP, βlg, and AP–βlg mixture samples at different concentrations. All samples were calculated on a weight percentage basis (wt%). Sodium azide (0.01 wt%) was added to the samples as an antimicrobial agent.

Three sample sets were prepared: a calibration set, a time set, and a prediction set.

The calibration set was used to obtain a model that can predict AP and βlg concentration of unknown samples from FT-IR absorbance spectra. The samples were prepared by weighing material from the stock solutions followed by rapid mixing. A volume of ~3–4 μL was taken immediately after mixing and placed into a liquid cell in order to avoid any possible phase segregation. The FT-IR spectrum was taken after 10 min.

The time set was used for finding out the time needed for reaching equilibrium and how the phase segregation evolves with time. Samples of more or less the same concentration were prepared, 5.4% AP and 16.8% βlg, and their spectra were taken at different periods of time (0 h to 6 weeks).

The prediction set was used for the construction of the AP–βlg–$D_2O$ phase diagram. AP–βlg mixture samples were left for a period of time to phase segregate and afterwards were centrifuged at 40,000 r.p.m. for 3 h. After centrifugation most samples appeared to be separated into different layers. A sample of each layer was collected and its spectrum was taken.

$D_2O$ was used as a solvent instead of $H_2O$ because the water has strong absorption bands that, by overlapping, mask the bands of AP and βlg.

### 2.3. Fourier transform-infrared spectroscpy (FT-IR)

FT-IR spectrum measurements of the AP–βlg–$D_2O$ samples were performed with a Bruker IFS 66 spectrometer (Bruker Optics GmbH, Ettlingen, Germany). A spectrum of the vacuum-tight empty liquid cell, supplied with $CaF_2$ windows (19 mm diameter) and spacer (12 μm thickness), was recorded and used as a background. Each spectrum was recorded between 600 and 4000 $cm^{-1}$ (even though the spectral range used for further analysis was only between 980 and 2000 $cm^{-1}$) at a resolution of 4 $cm^{-1}$, with 100 accumulative scans. The spectrometer was purged with dry nitrogen for 10 min prior to measurement.

The equipment was checked by contrasting the peak of the $CO_2$-specific peak at 2349 $cm^{-1}$, and sample spectra were normalized by setting the lowest absorbance in the range between 980 and 2000 $cm^{-1}$ and finally scaling the $D_2O$ peak at 1210 $cm^{-1}$ to an absorbance of unity.

Partial Least Square (PLS) analysis was applied to the spectra data to find a model that explained the relationship

between the spectra and the concentration of AP, βlg, and $D_2O$ in the samples and this model, which was cross-validated, was used to predict the composition of the phases of the phase-segregated samples. PLS was performed with The Unscrambler software (version 9.0, CAMO Process AS, Oslo, Norway).

The quality of the model, fully cross-validated, was assessed by looking at the score plot, loading plot, residual variance plot, regression coefficients plots, and predicted vs. measured plots and statistics such as RMSEP (Root Mean Square Error of Prediction), Bias, SEP (Standard Error of Performance), RMSEC (Root Mean Square Error of Calibration), SEC (Standard Error of Calibration), defined as:

$$\mathrm{RMSEP} = \sqrt{\frac{\sum_{i=1}^{n}(\hat{y}_i - y_i)^2}{n}} \quad (1)$$

$$\mathrm{Bias} = \frac{\sum_{i=1}^{n}(\hat{y}_i - y_i)}{n} \quad (2)$$

$$\mathrm{SEP} = \sqrt{\frac{\sum_{i=1}^{n}(\hat{y}_i - y_i - \mathrm{Bias})^2}{n-1}} \quad (3)$$

$$\mathrm{RMSEP}^2 \approx \mathrm{SEP}^2 + \mathrm{Bias}^2 \quad (4)$$

where $\hat{y}_i$ is the predicted concentration, $y_i$ the original concentration and $n$ the number of samples for RMSEP and SEP, but $\hat{y}_i$ is the modeled concentration for RMSEC and SEC.

### 2.4. X-ray powder diffraction (XR-PD)

A synchrotron (Beamline I911-5 Segin, from MAX-lab, Lund University, Lund, Sweden) was used for checking the retrogradation of AP in the phase-segregated samples rich in AP. The wavelength of the synchrotron was fixed at 0.907 Å and the beam was first monochromatized and horizontally focused by a bent silicon crystal working in Bragg geometry and then focused vertically by a 400 mm, curved multi-layer mirror. The high-flux photon beam was produced by a super-conducting multi-pole wiggler.

The synchrotron was checked with lanthanum hexaboride crystal ($LaB_6$).

By scooping, the sample was placed on a loop sample holder with a diameter between 0.5 and 0.7 mm and set at 35.2 mm from the MARCCD detector (Mar Research GmbH, Norderstedt, Germany). Data were collected for 30 s at room temperature.

The powder images were analyzed with Fit2D software (version 12.077, Andy Hammersley, ESRF), and the intensities in the $2\theta$ range (0° and 72.9°) were integrated. The synchrotron data were collected at $\lambda = 0.907$ Å, but for comparison reasons the data were changed to $\lambda = 1.54$ Å (Cu-$K_\alpha$) by using the following equation:

$$\theta_{\lambda_2} = \arcsin\left[\frac{\lambda_2 * \sin\theta_{\lambda_1}}{\lambda_1}\right] \quad (5)$$

$\theta_{\lambda_1}$ and $\theta_{\lambda_2}$ are the diffraction angle at $\lambda_1 = 0.907$ and $\lambda_2 = 1.54$, respectively.

### 2.5. Differential scanning calorimetry (DSC)

DSC 6200 from Seiko Instruments Inc., Minato, Tokyo, Japan, was used for the evaluation of the retrogradation of AP in the phase-segregated samples rich in AP. The DSC was calibrated using indium, and an empty pan was used as a reference. The sample was placed in a weighed coated aluminum pan which was sealed and reweighed and heated from 20 to 150 °C at 10 °C/min. The dry matter content was determined by leaving the sample at 105 °C for 16 h. The data were evaluated using the EXSTAR 6000 Thermal Analysis System software provided by the manufacturer of the instrument.

## 3. Results

FT-IR spectra of AP, βlg, and AP–βlg solutions were collected. Typical spectra are shown in Fig. 1. An FT-IR spectrum is composed of specific bands that correspond to the skeletal structure (fingerprint) and functional groups (e.g. C=O, N–H, C≡N) of the sample. AP displays specific bands in regions I and III of the spectrum; most pronounced are the saccharide bands (953–1180 $cm^{-1}$) in region I (Pavia, Lampman, & Kriz, 2001, chap. 2). The strong band in region II corresponds to $D_2O$. βlg displays bands in regions II, III, and IV of the spectrum that correspond to features in the secondary structure of the protein (α-helix, β-sheet, β-bend, β-turn, and random coil) usually known as Amide I (1600–1700 $cm^{-1}$), Amide II (1600–1400 $cm^{-1}$), and Amide III (1200–1400 $cm^{-1}$). These signals correspond to the stretching and bending vibration of C=O, C–N, C–C–N, N–H, C–O, C–C, and the signal of the Amide III is weak (Barth & Zscherp, 2002). The bands in region III are a result of the contribution of AP

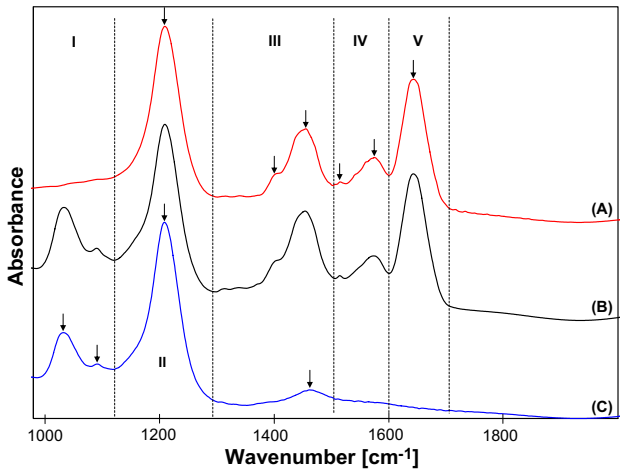


Fig. 1. Fourier transform infrared spectra of three samples of the calibration set: (A) βlg–$D_2O$ sample (14.19% βlg); (B) AP–βlg–$D_2O$ sample (7.58% AP and 13.61% βlg); and (C) AP–$D_2O$ sample (6.68% AP).

and βlg bands, therefore demonstrating the importance of having AP–βlg–$D_2O$ mixture samples in the calibration set.

$H_2O$ content in the samples was less than 2% and, as impurity, did not disturb the bands within the selected wave number range below ~2%.

### 3.1. PLS model for AP–βlg–$D_2O$ system

A calibration set of AP–βlg–$D_2O$ samples was measured and analyzed using PLS analysis to establish the relationship between the FT-IR spectra and the composition. The concentration of polysaccharide and protein in the calibration-set samples covered almost the complete concentration range expected for AP and βlg in the phase-segregated samples (see Fig. 2).

AP and βlg concentration as a function of the FT-IR spectra were modeled simultaneously using a PLS analysis (Esbensen, 2002, chaps. 6, 7, and 11). The concentrations of both macromolecules were obtained as the responses, and the spectra were used as the predictors.

The PLS model suited our system well. The regression coefficients agreed well with the spectral information from AP, βlg, and $D_2O$ (see Figs. 3 and 4).

No outliers or systematic errors were identified and the residuals were randomly scattered. The prediction was optimized using three components (three PCs). The PLS model has more or less the same response for the prediction of AP and βlg, though the correlation between the measured and predicted values for βlg is little bite better than for AP, see Figs. 3 and 4B. The error (RMSEC/RMSEP), precision (SEC/SEP), and accuracy (Bias) for modeling and prediction of the polysaccharide and protein were more or less in the same order of magnitude, see Table 1.

### 3.2. Evolution of the phase segregation of AP–βlg–$D_2O$ system

Samples of AP–βlg–$D_2O$ were prepared according to the methodology section. Care was taken to ensure that the AP

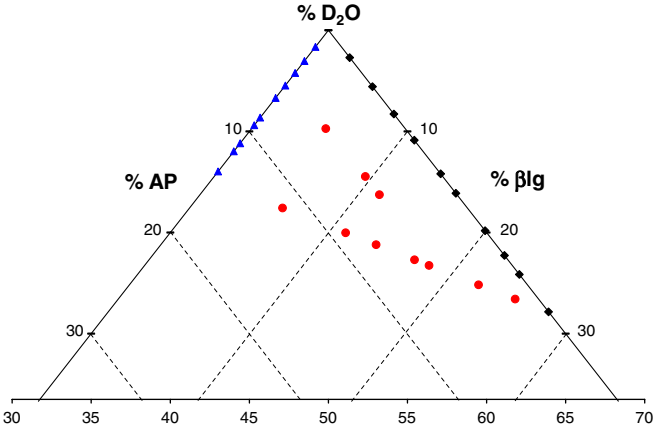


Fig. 2. Calibration set: (▲) AP–$D_2O$ samples; (◆) βlg–$D_2O$ samples; and (●) AP–βlg–$D_2O$ samples.

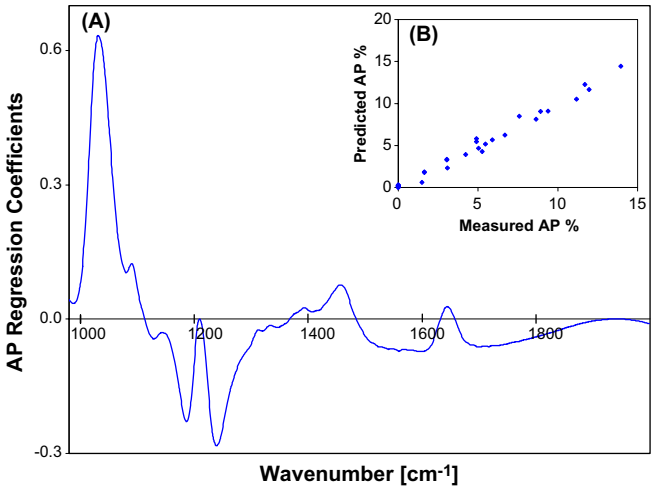


Fig. 3. (A) AP regression coefficient plot, numerical coefficients that express the link between variation in the spectrum and AP concentration and (B) AP concentration predicted vs. measured plot.

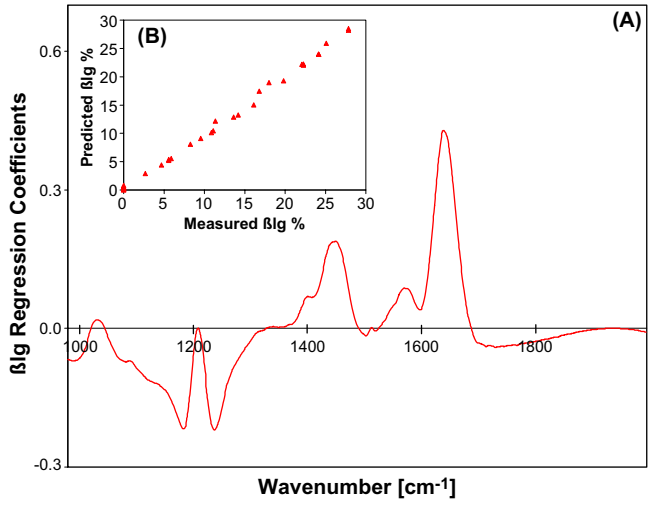


Fig. 4. (A) βlg regression coefficient plot, numerical coefficients that express the link between variation in the spectrum and βlg concentration and (B) βlg concentration predicted vs. measured plot.

Table 1
PLS model fit measures

| | Calibration | | Prediction | |
|---|---|---|---|---|
| | AP | βlg | AP | βlg |
| RMSEC/RMSEP | 0.43 | 0.55 | 0.39 | 0.50 |
| SEC/SEP | 0.43 | 0.56 | 0.40 | 0.51 |
| Bias | $3 \cdot 10^{-3}$ | $-4 \cdot 10^{-3}$ | $2 \cdot 10^{-7}$ | $-6 \cdot 10^{-8}$ |

was fully dissolved and that all immediate precipitates as well as eventual insoluble fragments from both the AP and the βlg solutions were removed before the samples were made. The samples were then weighed together, mixed and allowed to equilibrate for 24 h. No signs of spontaneous segregation in layers were seen (Fig. 5A). At low macromolecular concentration, samples appeared clear; however, at increasing macromolecular concentration they

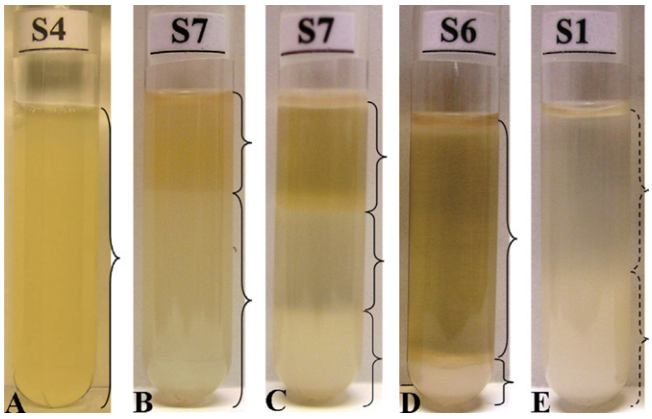


Fig. 5. AP–βlg–$D_2O$ photos: (A) before phase segregation and centrifugation, 5.64% AP and 16.44% βlg; (B) after phase segregation and before centrifugation, 5.90% AP and 17.43% βlg; (C), (D), and (E) after phase segregation and centrifugation at 40,000 r.p.m. for 3 h, 5.90% AP and 17.43% βlg, 2.79% AP and 22.29% βlg, and 10.80% AP and 5.80% βlg, respectively. The braces ({}) indicate the boundaries between the layers.

appeared thick and turbid. The turbidity as well as the thickness increased with increasing AP content.

After 24 h of equilibration time, the samples started to seem phase-segregated (Fig. 5B) and the phase boundaries were enhanced when they were centrifuged (3 h at 40,000 r.p.m.). After centrifugation most samples separated into either two layers, one upper layer and one lower layer (Fig. 5D and E), or three layers (Fig. 5C). The third layer appeared (from its turbidity and consistency) to be a separation of the lower layer into two different layers.

The upper layer was yellowish and clear. The boundary between the upper layer and the lower layer or the intermediate layer appeared distinct, indicating a clear difference in refractive index. The intermediate layer appeared more or less transparent, see Fig. 5C, while the lower phase had a pronounced turbidity. The boundary between the intermediate layer and the lower layer was more gradual.

Typical FT-IR spectra of a sample with three layers can be seen in the Fig. 6, showing an upper layer rich in protein with low polysaccharide content, a lower layer rich in polysaccharide with low protein content and an intermediate layer with both macromolecules.

Although signs of segregation appeared after 24 h, there remained uncertainty about the time needed for reaching complete equilibrium. The time set sample of 5.4% AP and 16.8% βlg was monitored during 6 weeks to establish the equilibration time needed. AP and βlg concentration in the sample before as well as after equilibration and centrifugation can be seen in Figs. 7 and 8.

From the results, we may conclude that AP was already expelled from the upper layer after 24 h. At that moment, the AP content was around 2% and the βlg content around 21%. The intermediate layer was rich in both macromolecules, about 15% of βlg and about 6% of AP. There was a dramatic change in the AP and βlg content in the lower layer, changing from about 6% to 28% for AP and from about 17% to 3% for βlg.

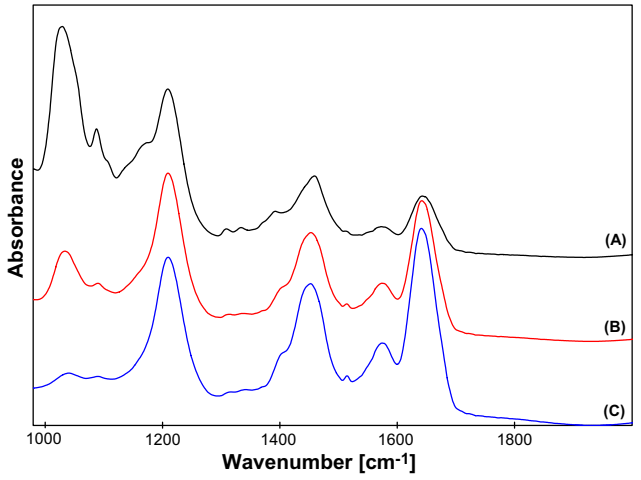


Fig. 6. Fourier transform infrared spectra of AP–βlg–$D_2O$ sample (5.64% AP and 16.44% βlg): (A) lower layer; (B) medium layer, and (C) upper layer.

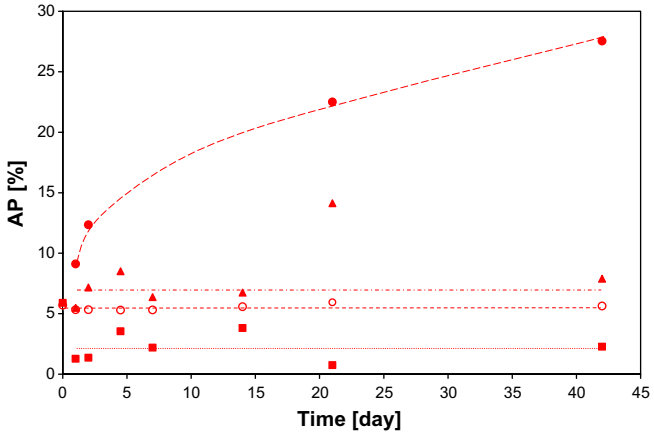


Fig. 7. AP concentration vs. time: (○) AP concentration in the original mixture sample, prior equilibration; (■) AP concentration in the upper layer; (▲) AP concentration in the intermediate layer; and (●) AP concentration in the lower layer.

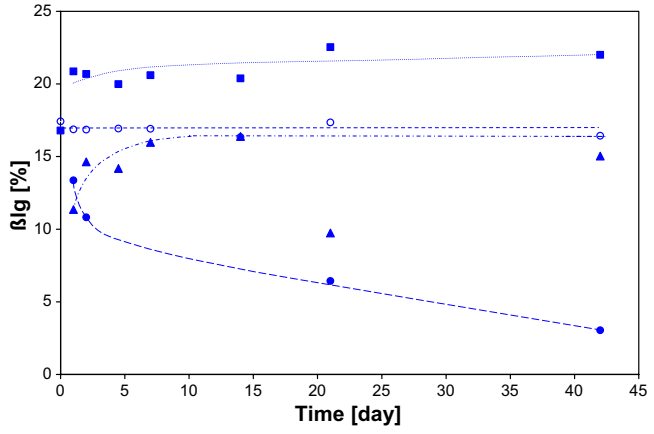


Fig. 8. βlg concentration vs. time: (○) βlg concentration in the original mixture sample, prior equilibration; (■) βlg concentration in the upper layer; (▲) βlg concentration in the intermediate layer; and (●) βlg concentration in the lower layer.

The concentration of the intermediate layer at 21 days of equilibration shows a discrepancy with the concentration of the samples at shorter (2–14 days) and longer (42 days) equilibration times, therefore this point has not been taken into consideration when the graphs were analyzed. Besides the concentration of the sample after 42 days of equilibration follows the general pattern presented in Fig. 11 relative to the composition of the metastable phase.

Fluctuations in the AP and βlg concentration have approximately the same order of magnitude as the expected error.

Due to gradual changes in the AP and βlg concentration in the lower layer, it was decided to divide the prediction set into two groups. The spectra of the first group were taken after 2 weeks and the spectra of the second group after 6 weeks.

### 3.3. Phase diagram of AP–βlg–$D_2O$

A phase diagram of AP–βlg–$D_2O$ was constructed by equilibrating samples of different compositions followed by centrifugal separation and compositional quantification of the layers using FT-IR.

At low concentrations (below 10% of both AP and βlg) the system appeared homogeneous even after centrifugation. The phase became clear and yellowish at higher βlg concentrations and lower AP concentrations. However, a small amount of precipitated material from the sample was settled at the bottom, looking like a whitish solid gel. As it seemed to increase when βlg concentration was increased, we interpreted it as aggregated βlg.

At high AP and βlg concentration the samples did not look clear before centrifugation and they separated into two or three layers after centrifugation.

The lower layer of the samples with three layers was quite thick and whitish. The volume of the lower layer was very similar independent of AP and βlg concentration. The volume of the intermediate layer varied in opposite proportion to the volume of the upper layer.

At higher βlg concentration and lower AP concentration the samples showed only two layers even after centrifugation (Fig. 5D). The lower layer in the presence of two layers appeared similar in character to the lower layer also when three layers appeared in the sample. The appearance of a third layer after centrifugation was an indication that AP underwent some kind of molecular rearrangement with consequent expulsion of $D_2O$ and βlg.

### 3.4. Retrogradation of AP in the lower layer

As retrogradation of starch is a well-known phenomenon it was obvious to assume that the gradual transition of the intermediate phase into a new structure was a process caused by the retrogradation of starch. As retrogradation involves re-crystallization processes, calorimetry and X-ray diffraction techniques have been used to evaluate it.

Samples of the lower layer, with AP content higher than 30%, were analyzed. The X-ray diffraction diagrams showed well-defined peaks indicating that the samples had developed some degree of crystallinity (Fig. 9).

In starch granules, amylopectin is the main crystalline component and is arranged in different crystalline structures with distinct X-ray-scattering peaks in the wide-angle range. Three characteristic diffraction patterns have been identified: A (cereal starches), B (tuber, high-amylose, and waxy starches), and C (smooth-seeded pea and various bean starches, this pattern is believed to be a superposition of A and B) (Zobel, 1988a). During gelatinization and pasting crystallinity is lost, however it can be regained in ageing gels and backed products through molecular reassociation (Biliaderis, 1998, chap. 4).

The peaks were identified, diffraction angle $(\theta)$ and $d$-spacing, as the typical peaks for the A- and B-type patterns. The weak intensity signals correspond to the A-type and the strong intensity signals to the B-type (see Table 2), besides the peaks of these structures other peaks were seen in the region between 15° and 25° ($\lambda = 0.907$ nm) but were not identified.

The retrogradation of AP in the AP-rich phases was also confirmed by DSC. Endotherms were detected in the range between 60 and 80 °C, for some samples the melting temperature range was wide and for others narrow (see Fig. 10). Even though in one of the thermograms a second endotherm has been seen we can not explain its origin because studies on amylopectin retrogradation showed only one endotherm at lower temperatures than the temperature of gelatinization (~70 °C) (Chang & Lin, 2007), a second endotherm has been seen but during gelatinization and at low water content (<50% of water) (Biliaderis, 1998, chap. 4; Liu, Yu, Xie, & Chen, 2006). The presence of β-lactoglobulin in these samples (<3%) could influence on the DSC results considering that during heating the protein undergoes to conformational changes in its structure until it denatures (~80 °C), at low heating rates a shoulder at 60 °C has been seen besides the denaturation endotherm (Hoffmann, van Miltenburg, & van Mil, 1997).

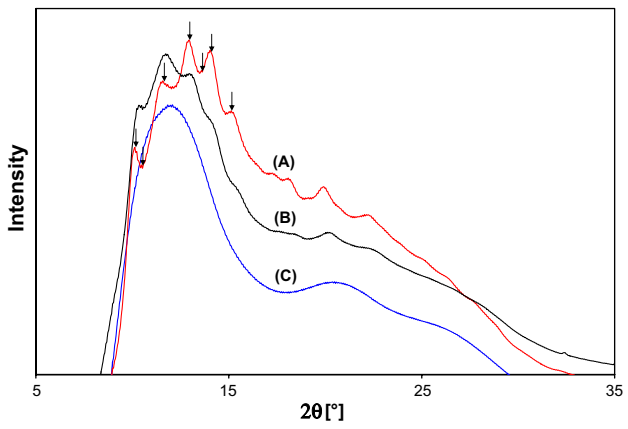


Fig. 9. X-ray powder diffraction of AP-rich samples: (A) and (B) lower layer, AP concentration around 30%, different degrees of crystallinity, and (C) amorphous sample prepared as a reference, AP concentration around 20%.

Table 2
XR-PD data of the lower phase of AP–βlg–$D_2O$ system and starch crystal forms A, and B as reference

| Peak number | Lower phase | | Starch type-A[a,b] | | Starch type-B[a,c] | |
|---|---|---|---|---|---|---|
| | $\lambda = 0.907$ Å | $\lambda = 1.54$ Å | $\lambda = 1.54$ Å | | $\lambda = 1.54$ Å | |
| | $2\theta$ (°) | $2\theta$ (°) | $2\theta$ (°) | $d$ (Å) | $2\theta$ (°) | $d$ (Å) |
| 1 | | | | | 5.8 | 15.22 |
| 2 | | | 15.3 | 5.78 | 15.3 | 5.78 |
| 3 | 10.1 | 17.4 s[d] | 17.4 | 5.09 | 17.3 | 5.12 |
| 4 | 10.5 | 18.0 w[e] | 18.3 | 4.84 | | |
| 5 | 11.6 | 19.9 | | | 20.1 | 4.41 |
| 6 | 12.9 | 22.3 s | | | 22.7 | 3.91 |
| 7 | 13.6 | 23.5 w | 23.5 | 3.78 | | |
| 8 | 14.0 | 24.3 s | | | 24.5 | 3.63 |
| 9 | 15.0 | 26.1 | 26.4 | 3.37 | 26.9 | 3.31 |

*Note:* [a]Zobel (1988a,b); [b]Cheetham and Tao (1998); [c]Cleven, van der Berg, and van der Plas (1978); [d]strong diffraction intensity signal; [e]weak diffraction intensity signal.

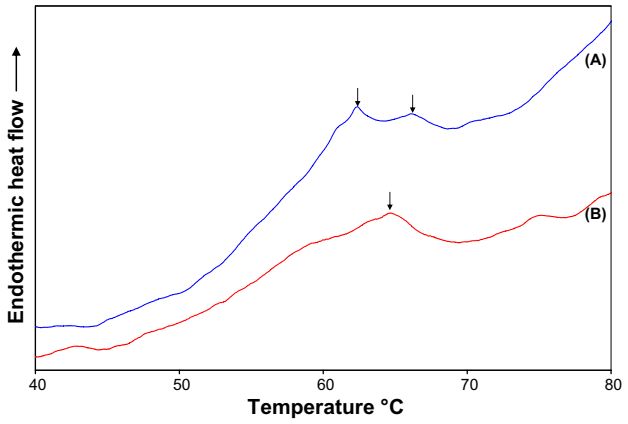


Fig. 10. DSC thermograms for AP-rich-lower layer, AP content higher than 30%. (A) Two endotherms and wide melting temperature range and (B) one endotherm and narrow melting temperature range.

## 4. Discussion

In the study of the phase segregation of a polysaccharide–protein system, the FT-IR spectroscopy technique in combination with PLS analysis worked well because the spectral difference among AP, βlg, and $D_2O$ are clear and a good correlation between concentration and spectral response can be obtained.

### 4.1. AP–βlg–$D_2O$ phase segregation

The layers after centrifugation in the results section are interpreted as representing the equilibrium or semi-equilibrium concentrations of the respective phases. In phase-segregated samples the upper layer is interpreted as a βlg-rich phase and the lower phase is interpreted as an AP-rich phase in a sample undergoing a binodal phase separation. The phase behavior of AP–βlg–$D_2O$ system observed after two different equilibration times, 6 and 2 weeks, are illustrated in Figs. 11 and 12, respectively.

In most samples an intermediate layer is observed. We interpret this layer as being a metastable phase that slowly segregates into a stable protein-rich phase and a stable retrograded polysaccharide phase. The lower layer is interpreted as the retrograded phase because: (i) it grows with time, (ii) it has a low protein content, and (iii) it displays crystalline order. The lower layer appears white. It is difficult to exclude that the layer also contains domains of the metastable phase trapped in the retrograded network. Retrogradation in starch solutions has been studied by many scientists for instance, by Biliaderis (1998, chap. 4).

The metastable AP–βlg–$D_2O$ phase contains a high concentration of protein. The protein–polysaccharide ratio is 1.2 after 6 weeks and a bit closer to 1 after 2 weeks.

Both phase diagrams are very asymmetric; when looking at the segregation between the metastable phase and the protein-rich phases, the two-phase region is strongly shifted towards the protein-rich phase. The asymmetry and shifting are consistent with the behavior predicted for a mixture containing macromolecules of different molecular weight, the binodal being displaced towards the macromolecule of lower molecular weight, in this case βlg (Kalichevsky & Ring, 1987).

The retrograded phase contains only a small amount of protein and the phase diagram appears much more symmetric. The tie-lines (lines between co-existence phases) connect a protein-rich phase with high water content and an AP-rich phase with low water content; this can tentatively be interpreted as the retrograded phase having a stronger interpolymer interaction. The slope of the tie-lines changes which has been observed in other polysaccharide–protein systems as well, e.g. amylopectin–gelatin (Grinberg & Tolstoguzov, 1972; Durrani et al., 1993), amylopectin–casein (Antonov et al., 1977), and whey protein–dextran (Syrbe, Fernandes, Dannenberg, Bauer, & Klostermeyer, 1995).

Increasing the equilibration time of the AP–βlg–$D_2O$ system, the binodal of the polysaccharide-rich phase

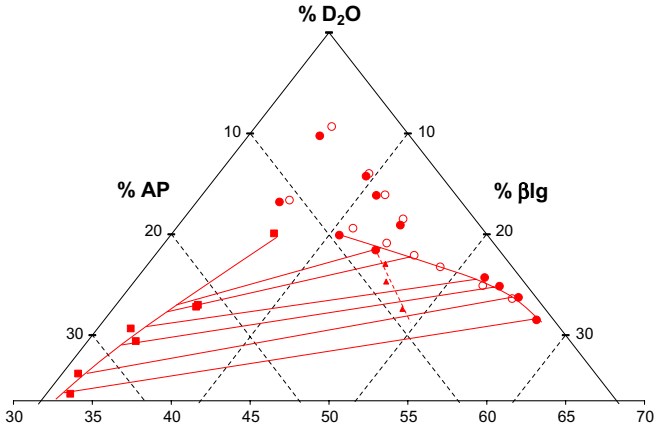


Fig. 11. AP–βlg–$D_2O$ phase diagram, equilibration time of 6 weeks: (●) concentration of the βlg-rich phase; (▲) concentration of the metastable phase; (■) concentration of the retrogradated AP-rich phase; (○) concentration of the original sample; (–) binodal and tie-lines; (---) line of the metastable phase.

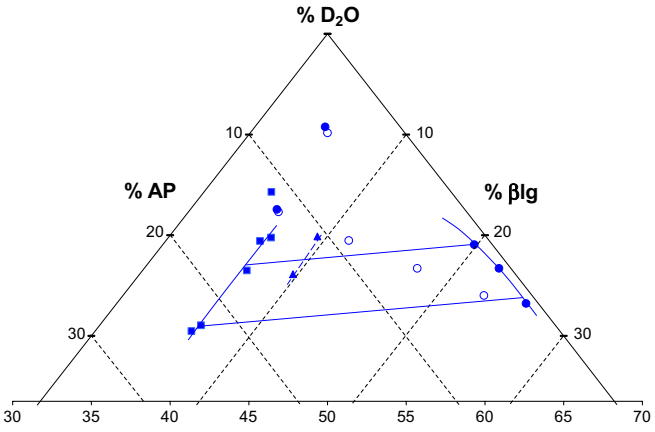


Fig. 12. AP–βlg–$D_2O$ phase diagram, equilibration time of 2 weeks: (●) concentration of the βlg-rich phase; (▲) concentration of the metastable phase; (■) concentration of the retrogradated AP-rich phase; (○) concentration of the original sample; (—) binodal and tie-lines; (---) line of the metastable phase.

shifted toward AP, increasing the area of the two-phase region on the phase diagram.

The big difference in molecular weight and size between AP and βlg drive toward phase segregation but the amount of AP in the system controls the kinetics of phase segregation. At low AP concentrations, the molecules are well-separated and free to move independently, as such, the solution viscosity is not high. However, with increasing concentration, a stage is soon reached at which the molecules begin to overlap and interpenetrate, and the viscosity increases very sharply (Morris, 1995).

For an AP–βlg–$D_2O$ system the phase separation threshold is above ~20% total macromolecular concentration, this value is quite high in comparison to the values for rigid, linear polysaccharides (below 2%), globular protein–polysaccharide mixtures (above 4%) and mixtures of globular proteins (exceeds 12%) (Tolstoguzov, 2000). However, it is important to mention that the phase segregation of these systems was mainly induced by heating, changing pH, and increasing ionic strength, which is not our case. In our system the native protein is considerable smaller than the polymer, the size of βlg is 4 nm in diameter (dimer form) (Sawyer, 2003, chap. 7) and the size of AP molecule is about 100–150 Å in diameter and 2000–4000 Å long (French, 1984, chap. VII), therefore the reduction of the conformation entropy is small and phase segregation occurs only at high concentrations, which is in accordance with the theory developed de Gennes (1979) and Odijk (1996, 1997) for these kind of systems where the size of the polymer is considerable larger than the colloidal particle.

### 4.2. Structural changes in the phases

During the equilibration time, structural changes occurred in the system mainly in the metastable phase where AP started to re-crystallize.

$D_2O$ and βlg are excluded from the metastable phase during AP re-crystallization, the degree of exclusion depends on the type of the crystal structure. The A-type structure (the most thermodynamically stable form) has a closely packed arrangement of double helices, whereas the B-type structure (kinetically preferred form) consists of a more open packing of helices with a correspondingly greater amount of inter-helical water. Thus, the B- to A-type transition could occur by a simple shifting of helices following removal of water. The A- to B-type transition is less favorable energetically (Gidley, 1987; Ring, 1985; Zobel, 1988b).

The stronger signals of the B- over the A-type suggest that AP with longer chain length started to retrograde because AP with short chain length (<20 residues) exhibit A-type crystallinity and AP with longer average chain length show the B pattern (Biliaderis, 1998, chap. 4).

The broad range of melting temperatures and having more than one endotherm are indicative of a wide range in the size and perfection of the crystals in the lower phase. The thermograms revealed the formation of a disproportionate number of poorer, less perfect crystals; the A-type crystals melt at higher temperature than B-type crystals do (Whittam, Noel, & Ring, 1990). The degree of crystallinity increases with time and AP concentration. The outer branches of AP are responsible for crystallinity due to the formation of double-helical junction zones, the crystallization of amylopectin is slow and could take many weeks (Miles, Morris, Orford, & Ring, 1985) even at sufficiently high AP concentration can form physically cross-linked thermoreversible gels upon cooling to below room temperature (Durrani & Donald, 1995).

## 5. Conclusions

Amylopectin and β-lactoglobulin phase segregate in one stable phase rich in protein and one metastable phase with about equal ratios between polysaccharide and protein. The metastable phase gradually separates into the protein-rich phase and the retrograded AP-rich phase.

Phase segregation is driven mainly by the difference in molecular interactions of the polysaccharide and protein. The difference in size makes the phase segregation very asymmetrical when the separation between the metastable phase and the protein-rich phase is considered. The difference in size is most likely also the cause as to why the phase segregation threshold is high.

AP retrogrades slowly and gradually with time in the polysaccharide-rich phase, and the degree of crystallinity is low.

## Acknowledgements

We are grateful to the Polymer and Materials Chemistry Division of Lund University for letting us to use the FT-IR spectrometer and to the National Electron Accelerator Laboratory for Synchrotron Radiation Research, Nuclear

Physics and Accelerator Physics (MAX-lab, Lund University), for letting us to use the synchrotron, Beamline I911-5.

Financial support was obtained from the Swedish International Development Agency (Sida/SAREC).

## References

Antonov, Yu. A., Grinberg, V. Ya., & Tolstoguzov, V. B. (1977). Phase equilibriums in water–protein–polysaccharide systems: II. Water–casein–neutral polysaccharide systems. *Colloid and Polymer Science, 255*(10), 937–947.

Barth, A., & Zscherp, C. (2002). What vibrations tell ass about proteins. *Quarterly Reviews of Biophysics, 35*(4), 369–430.

Biliaderis, C. G. (1998). Structure and phase transitions of starch polymers. In R. H. Walter (Ed.), *Polysaccharide association structures in food* (pp. 57–168). New York, USA: Marcel Dekker, Inc.

Cleven, R., van der Berg, C., & van der Plas, L. (1978). Crystal Structure of Hydrated Potato Starch. *Starch/Starke, 30*(7), 223–228.

Chang, Y.-H., & Lin, J.-H. (2007). Effects of molecular size and structure of amylopectin on the retrogradation thermal properties of waxy rice and waxy cornstarches. *Food Hydrocolloids, 21*(4), 645–653.

Cheetham, N. W. H., & Tao, L. (1998). Variation in crystalline type with amylose content in maize starch granules: An X-ray powder diffraction study. *Carbohydrate Polymers, 36*, 277–284.

Donald, A. M., Durrani, C. M., Jones, R. A. L., Rennie, A. R., & Tromp, R. H. (1995). Physical methods to study phase separation in protein–polysaccharide mixtures. In S. E. Harding, S. E. Hill, & J. R. Mitchell (Eds.), *Biopolymer mixtures* (pp. 99–116). Nottingham, UK: Nottingham University Press.

Durrani, C. M., Prystupa, D. A., Donald, A. M., & Clark, A. H. (1993). Phase diagram of mixtures in aqueous solution using Fourier infrared spectroscopy. *Macromolecules, 26*, 981–987.

Durrani, C. M., & Donald, A. M. (1995). Physical characterisation of amylopectin gels. *Polymer Gels and Networks, 3*(1), 1–27.

Esbensen, K. H. (2002). Multivariate calibration (PCR/PLS), validation: Mandatory performance testing & PLS (PCR) multivariate calibration – in practice. In K. H. Esbensen (Ed.), Multivariate data analysis – in practice (pp. 115–153, 155–168, 241–270). Esbjerg, Norge: CAMO Process AS.

French, D. (1984). Organisation of starch granules. In R. L. Whistler, J. N. BeMiller, & E. F. Paschall (Eds.), *Starch chemistry and technology* (pp. 183–247). London, England: Academic Press, Inc.

de Gennes, P. G. (1979). Colloid suspensions in a polymer solution. *Comptes Rendus des Seances de l'Academie des Sciences. Serie B: Sciences Physiques, 288*(21), 359–361.

Gidley, M. J. (1987). Factors affecting the crystalline type (A–C) of native starches and model compounds: A rationalization of observed effects in terms of polymorphic structures. *Carbohydrate Research, 161*, 301–304.

Grinberg, V. Ya., & Tolstoguzov, V. B. (1972). Thermodynamic compatibility of gelatin with some D-glucans in aqueous media. *Carbohydrate Research, 25*(2), 313–321.

Grinberg, V. Ya., & Tolstoguzov, V. B. (1997). Thermodynamic incompatibility of proteins and polysaccharides in solutions. *Food Hydrocolloids, 11*(2), 145–158.

Hoffmann, M. A. M., van Miltenburg, J. C., & van Mil, P. J. J. M. (1997). The suitability of scanning calorimetry to investigate slow irreversible protein denaturation. *Thermochimica Acta, 306*(1–2), 45–49.

Kalichevsky, M. T., & Ring, S. G. (1987). Incompatibility of amylose and amylopectin in aqueous solution. *Carbohydrate Research, 162*, 323–328.

Liu, H., Yu, L., Xie, F., & Chen, L. (2006). Gelatinization of cornstarch with different amylose/amylopectin content. *Carbohydrate Polymers, 65*(3), 357–363.

Manners, D. J. (1989). Recent developments in our understanding of amylopectin structure. *Carbohydrate Polymers, 11*(2), 87–112.

Miles, M. J., Morris, V. J., Orford, P. D., & Ring, S. G. (1985). The roles of amylose and amylopectin in the gelation and retrogradation of starch. *Carbohydrate Research, 135*(2), 271–281.

Morris, E. R. (1995). Polysaccharide rheology an in-mouth perception. In A. M. Stephen (Ed.), *Food polysaccharides and their applications* (pp. 517–547). New York, USA: Marcel Dekker.

Pavia, D. L., Lampman, G. M., & Kriz, G. S. (2001). Infrared spectroscopy. In D. L. Pavia, G. M. Lampman, & G. S. Kriz (Eds.), *Introduction to spectroscopy* (pp. 13–101). Washington, USA: Brooks/Cole, Thomson Learning Inc.

Piculell, L., Bergfeldt, K., & Nilsson, S. (1995). Factors determining phase behaviour of multi component polymer systems. In S. E. Harding, S. E. Hill, & J. R. Mitchell (Eds.), *Biopolymer mixtures* (pp. 13–35). Nottingham, UK: Nottingham University Press.

Odijk, T. (1996). Protein–macromolecule interactions. *Macromolecules, 29*(5), 1842–1843.

Odijk, T. (1997). Depletion around a protein sphere interacting with a semidilute polymer solution. *Langmuir, 13*(13), 3579–3581.

Olsson, C., Langton, M., & Hermansson, A.-M. (2002). Microstructures of b-lactoglobulin/amylopectin gels on different length scales and their significance for rheological properties. *Food Hydrocolloids, 16*(2), 111–126.

Olsson, C., Frigaard, T., Andersson, R., & Hermansson, A.-M. (2003). Effects of amylopectin structure and molecular weight on microstructural and rheological properties of mixed b-lactoglobulin gels. *Biomacromolecules, 4*(5), 1400–1409.

Ring, S. G. (1985). Observations on the crystallization of amylopectin from aqueous solution. *International Journal of Biological Macromolecules, 7*(4), 253–254.

Sawyer, L. (2003). b-Lactoglobulin. In P. F. Fox & P. L. H. McSweeney (Eds.), *Advanced dairy chemistry. Proteins* (Vol. I, pp. 319–385). New York, USA: Kluwer Academic/Plenum.

Simonet, F., Garnier, C., & Doublier, J.-L. (2000). Partition of proteins in the aqueous guar/dextran two-phase system. *Food Hydrocolloids, 14*(6), 591–600.

Syrbe, A., Fernandes, P. B., Dannenberg, F., Bauer, W., & Klostermeyer, H. (1995). Whey protein + polysaccharide mixtures: Polymer incompatibility and its application. In E. Dickinson & D. Lorient (Eds.), *Food macromolecules and colloids* (pp. 328–339). Cambridge, UK: Royal Society of Chemistry.

Tolstoguzov, V. B. (1986). Functional properties of protein–polysaccharide mixtures. In J. R. Mitchell & D. A. Ledward (Eds.), *Functional properties of food macromolecules* (pp. 385–415). London, UK: Elsevier Applied Science.

Tolstoguzov, V. B. (1993). Thermodynamic incompatibility of food macromolecules. In E. Dickinson & P. Walstra (Eds.), *Food colloids and polymers: Stability and mechanical properties* (pp. 94–102). Cambridge, UK: The Royal Society of Chemistry.

Tolstoguzov, V. B. (2000). Phase behavior of macromolecular components in biological and food systems. *Nahrung, 44*(2), 299–308.

Whittam, M. A., Noel, T. R., & Ring, S. G. (1990). Melting behaviour of A- and B-type crystalline starch. *International Journal of Biological Macromolecule, 12*(6), 359–362.

Zhang, G., & Foegeding, E. A. (2003). Heat-induced phase behavior of b-lactoglobulin/polysaccharide mixtures. *Food Hydrocolloids, 17*(6), 785–792.

Zobel, H. F. (1988a). Starch crystal transformations and their industrial importance. *Starch/Starke, 40*(1), 1–7.

Zobel, H. F. (1988b). Molecules to granules: A comprehensive starch review. *Starch/Starke, 40*(2), 44–50.